

# Three jet production and gluon saturation effects in p-p and p-Pb collisions within high-energy factorization

*A. van Hameren, P. Kotko, K. Kutak*

*The H. Niewodniczański Institute of Nuclear Physics*

*Polish Academy of Sciences*

*Radzikowskiego 152, 31-342 Cracow, Poland*

## Abstract

We analyze three-jet production in the central-forward and forward rapidity regions in proton-proton and proton-lead collisions at LHC energies. Our calculation relies on high-energy factorization with a single off-shell gluon obeying small  $x$  evolution equation which includes saturation. The calculations are made using two independent Monte Carlo codes implementing tree-level gauge invariant off-shell matrix elements. We calculate differential cross sections for azimuthal decorrelations and unbalanced jet transverse momenta and discuss them in the context of differences in the evolution of the unintegrated gluon densities.

## 1 Introduction

Jet production processes are excellent testing ground for perturbative QCD, notably because their analysis does not require a knowledge of fragmentation functions which are subject to large errors. The only non-perturbative input that enters theoretical calculations are thus parton distribution functions (PDFs). They are defined by a particular factorization scheme; for instance for the collinear factorization (see [21] for a review) the PDFs undergo linear Dokshitzer-Gribov-Lipatov-Altarelli-Parisi evolution equations. It is however known, that at high energies reachable nowadays at LHC, certain types of logarithms occurring in the perturbative calculations can spoil the procedure. The general method is to resum those logarithms giving rise to new types of evolution equations, for instance the linear Balitski-Fadin-Kuraev-Lipatov (BFKL) equation [42, 6], Catani-Ciafaloni-Fiorani-Marchesini (CCFM) [20, 14, 13], the nonlinear Balitski and Kovchegov (BK) equation [5, 40] or nonlinear extension of CCFM – the Kutak-Golec-Biernat-Jadach-Skrzypek (KGBJS) equation [44, 43].

An example of a situation that requires the resummation of high-energy logarithms is the production of forward jets [54, 25, 63, 51]. Large energies and rapidities of forward jets allows to probe the small  $x$  regime and thus it is an excellent testing ground for various resummation schemes and gluon saturation phenomenon which should occur at high-energy densities [32, 55]. Forward jets are even more attractive nowadays as it is possible to study them experimentally at LHC. Thanks to dedicated forward calorimeters, the ATLAS and CMS detectors allow to reconstruct large-transverse-momentum jets up to about 5 units of rapidity. This gives an opportunity to study small  $x$  effects experimentally and possibly access the kinematic region where gluon saturation may enter the game. There are indeed hints that saturation actually happens [61, 1, 28, 46]. Various studies of forward jets were done in Refs. [23, 24, 35, 17, 33]. For the recent experimental studies see [18, 37, 19].

In the present paper we study three-jet production at the LHC within the high-energy factorization framework, which shall be reviewed in Section 2. Multijet processes are interesting particularly due to a bigger phase space – by applying various cuts different properties of gluon densities can be studied. For instance by restricting two of the jets to balance each other on the transverse plane, the third jet can access the gluon transverse space directly. The detailed kinematics of the processes we consider is described in Section 3. We present numerical results and discuss their possible interpretation in Section 4. Finally, we give overall summary in Section 5.

## 2 Factorization at high energies

Let us now briefly recall some of the existing formalisms that may be attempted to describe the observables at high energies. Before doing so, let us however make some important remarks. First of all, the full control over the calculation, in particular over its limitations, can be achieved only when working within well established factorization theorems of QCD. Besides the well-known collinear factorization there are so-called transverse momentum dependent (TMD) factorization theorems. They do work in certain processes (see [21]) but fail in some other. In general they are expected to fail in hadron-hadron collisions ([22, 58], see also the short summary in [56]). The TMD factorizations involve transverse momentum dependent gluon distribution functions, similar to those that are often used in high-energy phenomenology. The problem is, however, that the former are not universal (this is the reason the factorization is violated) whereas the latter are often conjectured to be universal. Let us thus comment on the factorization at the kinematic limit we consider in the paper, namely the “small  $x$ ” regime. It deals with dense hadronic matter (especially for collisions with heavy ions) for which the formalism of Color Glass Condensate (CGC) [31] proves to be very successful [1]. Basically the TMD factorizations do not deal with the small  $x$  limit, although it was shown in [66] that the universality of TMD PDFs is also violated in that limit. On the other hand, in Ref. [27] it is argued that an “effective” factorization within CGC (for dilute-dense collisions) can be seen as an instance of TMD factorization in case of dijets production in the limit of small unbalanced transverse momentum. The factorization formula is then stated as a convolution of a few universal transverse momentum dependent gluon densities and matrix elements which are on-shell, but use off-shell kinematics. In large  $N_c$  limit those different gluon PDFs can be expressed in terms of two fundamental quantities: the Weizsäcker-Williams gluon density [52, 53] and the “dipole” gluon density (see eg. [41, 38] and references therein; for the possible theoretical issues of those gluon densities as seen from the TMD factorization point of view see [3, 4]). Both densities are related to certain two-point Green functions. In the more general case of multi-particle production higher correlators are needed (within CGC they are expressed by means of certain averages of the Wilson lines). However, as shown in Ref. [26] in case of dilute-dense collisions and large  $N_c$  limit only two-point and four-point Green functions are needed. For recent applications to multi-particle production see also [34].

We see, that the theoretical picture of the processes at very large densities (very small  $x$ ) is complicated. Unless one is outside the saturation regime (i.e. in the BFKL or CCFM domain), only simple cases like inclusive gluon production can be described in terms of single transverse momentum dependent gluon density [7, 30].

In the present paper we mainly concentrate on the proton-proton collisions within the kinematic region accessible by contemporary experiments. The nonlinear effects – although present – are actually rather weak. Therefore, we shall use simple  $k_T$ -factorization with a single type of unintegrated gluon density, incorporating, however, the nonlinear evolution (when necessary we shall compare the results to the BFKL evolution with sub-leading corrections included [48]). Although simplified, such an approach was proved to be very interesting phenomenologically [46].

As a reference for the  $k_T$ -factorization we take the works of Catani, Ciafaloni and Hautmann (CCH) [10, 11, 9, 15, 12, 16] (the following type of factorization formula appeared also much earlier in [32]). Originally it was stated for heavy quark pair production at tree-level; however we shall assume that one can extend it for more complicated final states including gluons, with the complications explained below. The factorization is expressed by the following formula (see Fig. 1A); for some partonic final state  $X$  and two initial state hadrons  $A, B$  we have

$$d\sigma_{AB \rightarrow X} = \int \frac{d^2 k_{T A}}{\pi} \int \frac{dx_A}{x_A} \int \frac{d^2 k_{T B}}{\pi} \int \frac{dx_B}{x_B} \mathcal{F}_{g^*/A}(x_A, k_{T A}) \mathcal{F}_{g^*/B}(x_B, k_{T B}) d\hat{\sigma}_{g^* g^* \rightarrow X}(x_A, x_B, k_{T A}, k_{T B}), \quad (1)$$

where  $\mathcal{F}_{g^*/H}$  are transverse-momentum-dependent densities of the off-shell gluons  $g^*$  inside  $H$  (to be discussed below) and  $\hat{\sigma}_{g^* g^* \rightarrow X}$  is the high-energy hard cross section for the process  $g^*(k_A) g^*(k_B) \rightarrow X$ . The momenta of the off-shell gluons that enter the hard cross section are defined to be

$$k_A^\mu = x_A p_A^\mu + k_{T A}^\mu, \quad k_B^\mu = x_B p_B^\mu + k_{T B}^\mu, \quad (2)$$

where  $p_A \cdot k_T = p_B \cdot k_T = 0$ . The hard amplitude with the external off-shell gluons is defined by means of certain high-energy (or eikonal) projectors, i.e. the off-shell leg (including the propagator)

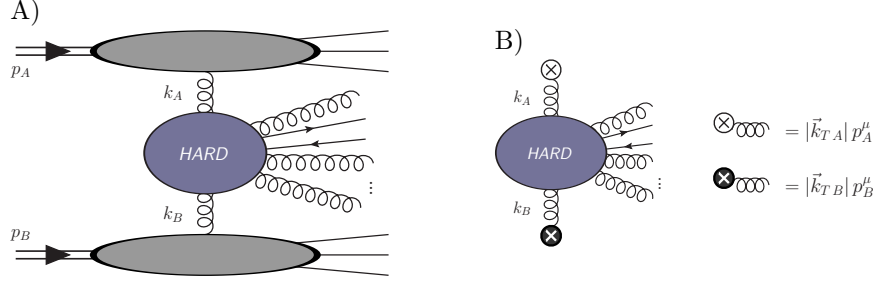


Figure 1: A) Factorization of a hadronic collision into unintegrated PDFs (top and bottom blobs after 'squaring') and parton-level sub-process (middle blob). B) The hard sub-process is defined by an off-shell matrix elements with incoming off-shell gluon propagators contracted with high-energy projectors (explained on the r.h.s). In order to make this amplitude gauge invariant additional contributions are needed (see the main text).

with momentum  $k_A, k_B$  is contracted with  $|\vec{k}_{T A}| p_A^\mu, |\vec{k}_{T B}| p_B^\mu$  respectively (see Fig. 1B). As already mentioned, in the original CCH works the production of a heavy quark pair was considered. In that case the corresponding off-shell amplitude is gauge invariant, fundamentally due to the form of the projectors. This is however not true for the off-shell amplitudes with gluons in the final state. There are several ways to deal with this problem. First, Lipatov's effective action [50] and the resulting Feynman rules [2] can be used. This is because the kinematics (2) corresponds to quasi-multi-Regge kinematics in the terminology of [2] (for recent LHC-related calculations in that framework we refer e.g. to [57, 59, 39]). A second approach developed recently in [65] is suitable for automatic calculation of large final state multiplicities and uses a manifestly gauge invariant method of embedding the off-shell process in a larger on-shell process without compromising high-energy kinematics. Finally, there is one more approach [64] suitable in a simplified situation described later in this section.

In the CCH approach, the transverse-momentum-dependent gluon densities  $\mathcal{F}_{g^*/H}$  were originally assumed to undergo the BFKL evolution. As we have remarked above, we shall use the formula (1) with  $\mathcal{F}_{g^*/H}$  incorporating more subtle effects, in particular gluon saturation. In the present paper we shall use the nonlinear BK equation, extended with a consistency constraint, a non singular piece of the gluon splitting function and running strong coupling constant [45, 47]. The strength of the non-linearity is adjusted by a parameter that can be interpreted as a radius of a hadron, either proton or nuclei (e.g. in Ref. [46] it was applied for a lead target). Let us remark, that since there is a conjecture that integration of  $\mathcal{F}_{g^*/H}$  over transverse momentum is related to a collinear PDF, we shall often refer to  $\mathcal{F}_{g^*/H}$  as the unintegrated gluon density. The relation between both quantities reads

$$\int dk_{T A}^2 \mathcal{F}_{g^*/A}(x_A, k_{T A}) = x_A f_{g/A}(x_A). \quad (3)$$

Suppose now, that we deal with asymmetric kinematics, i.e.  $x_B \gg x_A$ , which is a characteristic feature of forward scattering (see the next section). Then the gluon originating from hadron  $B$  is probed near the mass-shell and  $\mathcal{F}_{g^*/B}$  should be replaced by its collinear equivalent  $f_{g/B}$ . Moreover, the valence quarks play important role. Thus, the proper formula in such a setup is given by

$$d\sigma_{AB \rightarrow X} = \int \frac{d^2 k_{T A}}{\pi} \int \frac{dx_A}{x_A} \int dx_B \sum_b \mathcal{F}_{g^*/A}(x_A, k_{T A}) f_{b/B}(x_B) d\hat{\sigma}_{g^* b \rightarrow X}(x_A, x_B, k_{T A}), \quad (4)$$

where  $b$  runs over gluon and all the quarks that can contribute to the production of multiparticle state  $X$  (see also Ref. [23] and the appendix of [10] for the collinear limit in the high-energy factorization). In the formula above, any scale dependence was suppressed. The off-shell gauge invariant process  $g^* b \rightarrow g \dots g$  can be calculated along the lines of Ref. [64]. The case with

quarks is actually straightforward, as in axial gauge any gauge contribution due to Slavnov-Taylor identities vanishes.

Let us summarize our basic assumptions. We use  $k_T$ -factorized, hybrid (i.e. collinear PDF is mixed with the unintegrated one, see also [29] for CGC approach) form given in Eq. (4) with the inclusion of non-linear effects in the evolution of the unintegrated gluon PDF. The hard matrix elements are calculated fully off-shell at tree-level; they are gauge invariant, and all of them are convoluted with the same gluon density given in fundamental color representation, as given in [46].

### 3 Process definition and kinematics

Let us now give a detailed description of the process we are interested in. We want to study exclusive three jet events, namely,

$$A(p_A) B(p_B) \rightarrow J_1(p_1) J_2(p_2) J_3(p_3), \quad (5)$$

where  $A = \{p^+, \text{Pb}\}$ ,  $B = p^+$  and  $J_i(p_i)$  denotes the jet with momentum  $p_i$ . We work in the c.m. frame throughout the paper. This frame corresponds to LAB frame for  $p^+p^+$  collision, but not for the  $p^+ \text{Pb}$  collisions. In our frame we define

$$p_A^\mu = (E, 0, 0, -E), \quad p_B^\mu = (E, 0, 0, E), \quad (6)$$

with  $E = \sqrt{S}/2$  where  $S$  is the total c.m. energy squared. In the present paper we consider c.m. energies  $\sqrt{S} = 5.02 \text{ TeV}$  and  $\sqrt{S} = 7.0 \text{ TeV}$ .

Let us now discuss the kinematic cuts that are relevant to the physics we would like to address. To this end let us decompose the final state momenta as follows

$$p_i^\mu = \frac{|\vec{p}_{T i}|}{\sqrt{S}} (e^{\eta_i} p_A^\mu + e^{-\eta_i} p_B^\mu) + p_{T i}^\mu, \quad (7)$$

where  $p_{T i} \cdot p_A = p_{T i} \cdot p_B = 0$  and the rapidity  $\eta_i$  is defined as

$$\eta_i = \frac{1}{2} \ln \frac{p_i^0 + p_i^z}{p_i^0 - p_i^z}. \quad (8)$$

Further we note that

$$p_{T i}^\mu = (0, \vec{p}_{T i}, 0) \quad (9)$$

and

$$\vec{p}_{T i} = (|\vec{p}_{T i}| \sin \phi_i, |\vec{p}_{T i}| \cos \phi_i). \quad (10)$$

Now let us come back to the kinematic cuts. First of all we assume that

$$|\vec{p}_{T i}| > p_{T \text{ cut}}, \quad i = 1, 2, 3. \quad (11)$$

The actual values of the cuts shall be given in the following sections when we discuss numerical results. Typically, we shall order the jets with decreasing  $|\vec{p}_{T i}|$  values, i.e.

$$|\vec{p}_{T 1}| > |\vec{p}_{T 2}| > |\vec{p}_{T 3}|. \quad (12)$$

Further restriction is given by a jet definition. Here we work with anti- $k_T$  clustering algorithm [8] with radius  $R_{\text{cut}}$ , thus the final state momenta cannot be too close in the  $\phi - \eta$  space<sup>1</sup>. In order to access the small  $x$  region we have to impose additional cuts. According to (7) and the factorization formula (cf. Eq. (2)), the longitudinal fractions of the hadrons' momenta  $x_A, x_B$  that initiate the hard scattering are given by

$$x_A = \sum_i \frac{|\vec{p}_{T i}|}{\sqrt{S}} e^{\eta_i}, \quad x_B = \sum_i \frac{|\vec{p}_{T i}|}{\sqrt{S}} e^{-\eta_i}. \quad (13)$$

---

<sup>1</sup> Actually for tree-level parton-level processes it is equivalent to a proper cut on the  $\phi - \eta$  plane.

Thus, in order to select small, say,  $x_A$  for the fixed  $S$  and  $|\vec{p}_{Ti}|$  we have to go to large rapidity values, ideally for all the jets. In the same time  $x_B$  would be large; thus, this sort of kinematics is often referred to as *asymmetric kinematics*. If some of the jets appear in the central rapidity region, we can still access small  $x$  regime provided at least one of the jets is in the forward region. Those issues shall be illustrated by a specific calculation in Section 4.2. The forward region is defined as

$$\eta_{f0} \leq \eta_i \leq \eta_{f1}, \quad (14)$$

while the central region is defined as

$$|\eta_j| \leq \eta_c \quad (15)$$

with specific boundary values  $\eta_{f0}$ ,  $\eta_{f1}$ ,  $\eta_c$  given later. Note, that we tag the forward jet in the positive rapidity hemisphere only, both for proton-proton and proton-lead collisions.

There are also additional cuts that might be interesting for the studies of unintegrated gluon densities. We may restrict the two leading jets to be back-to-back-like. More precisely, we can define

$$p_{T12} = |\vec{p}_{T1} + \vec{p}_{T2}| < D_{\text{cut}}, \quad (16)$$

with  $D_{\text{cut}}$  parameter being not much smaller than  $p_{T\text{cut}}$ . Such a study is motivated by the fact, that for  $D_{\text{cut}} \rightarrow 0$  the total transverse momentum of the initial state gluons is transferred to the forward jet.

## 4 Numerical results and discussion

### 4.1 Preliminary remarks

The numerical calculations were performed using two new Monte Carlo programs and were cross-checked against each other. The first program is a C++ code using the **foam** algorithm [36] and based on the method for off-shell matrix elements described in Ref. [64]. The working-name of the program is **LxJet**<sup>2</sup>. The second independent code is a **fortran** program based on [65]. Since we want to study some small  $x$  properties of the jet observables within high-energy factorization itself, we do not interface the program with any parton shower in the present calculation. The final state parton shower can be added using e.g. **pythia** [60] and shall be done in the future. Another shortcoming comes from neglecting multiple parton interactions (MPIs). In the contrary to dijet production, where MPIs lead to a change of the overall normalization of angle distributions [62], the situation for three-jet production is more complicated and is left for further study.

Let us now summarize the inputs we have used. For the unintegrated parton densities  $\mathcal{F}_{g^*/H}$  we take the ones described in the previous section and fitted to HERA data in [46]. These include the nonlinear PDFs for proton, lead, and additionally the proton PDF with linear evolution [48]. For the collinear PDFs  $f_a$  we take CTEQ10 NLO set [49]. The consistent strong coupling constant is also taken from the same source. Since our calculations are essentially tree-level as far as the parton-level amplitude is concerned, there is a large dependence on the choice of the scales. In order to estimate the theoretical uncertainty we do the following standard procedure. First we set the renormalization and collinear factorization scales to be equal  $\mu_f = \mu_r \equiv \mu$  and choose

$$\mu = E_1 + E_2 + E_3. \quad (17)$$

Our error estimate is then given by the band constructed from the two outputs with the two choices of the scale (including statistical errors):  $\mu/2$  and  $2\mu$ . In all calculations we choose the radius of the anti- $k_T$  algorithm to be  $R_{\text{cut}} = 0.5$ .

We consider two rapidity configurations:

- *central-forward region*: we demand that the two hardest jets (with indices 1,2) are in the central region defined by  $\eta_c = 2.8$ , while the softest jet (with index 3) is in the forward region defined by  $\eta_{f0} = 3.2$ ,  $\eta_{f1} = 4.7$ ,
- *forward region*; all three jets are within the region defined by  $\eta_{f0} = 3.2$ ,  $\eta_{f1} = 4.9$ .

---

<sup>2</sup>The program shall be publicly available.

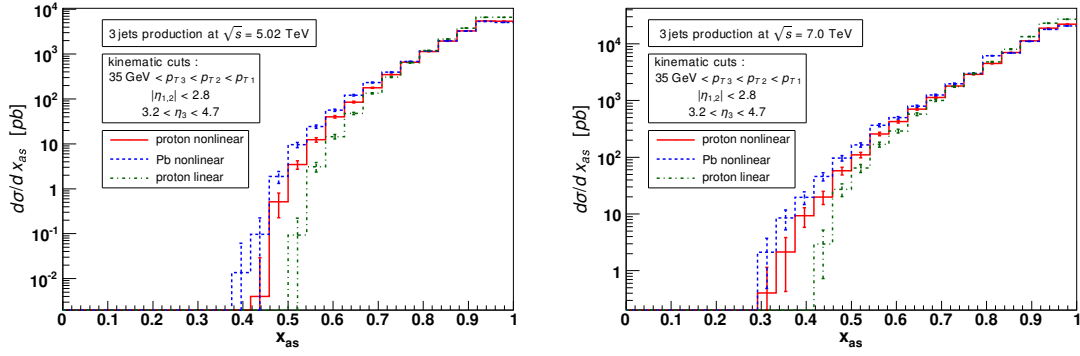


Figure 2: The differential cross section as a function of asymmetry variable  $x_{as}$  for the forward-central rapidity region and two different c.m. energies: left for 5.02 TeV, right for 7.0 TeV.

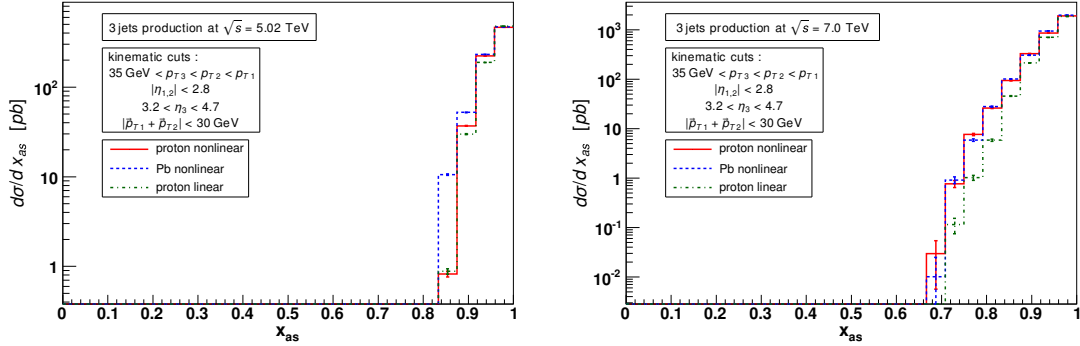


Figure 3: The differential cross section as a function of asymmetry variable  $x_{as}$  for forward-central rapidity region with back-to-back cut  $D_{cut} = 30$  GeV and two different c.m. energies: left for 5.02 TeV, right for 7.0 TeV.

## 4.2 Asymmetry distributions

In order to check if the region of the longitudinal fractions  $x_A$ ,  $x_B$  we access is consistent with our assumptions leading to Eq. (4) let us we define the following variable

$$x_{as} = \frac{|x_A - x_B|}{x_A + x_B}. \quad (18)$$

It has the support in  $[0, 1]$  and measures the asymmetry of the event (for  $x_{as} \rightarrow 1$  we have totally asymmetric events). We expect that within our kinematic cuts the cross section is dominated by asymmetric events, being thus in agreement with Eq. (4). This point shall be verified by explicit calculations below.

In the figures 2-4 we present differential cross sections in  $x_{as}$  for three different scenarios: forward-central rapidity region, forward-central region with two leading jets being close to back-to-back, and the purely forward region. The rapidity regions were defined in the previous section. Further details are given in the plots. We see that the collisions in the forward region (Fig. 4) are completely asymmetric as one should expect. However, most of the events in forward-central region are also asymmetric, as seen in Fig. 2. We have observed, that – as far as forward-central collisions are concerned – lowering the  $p_{T\text{ cut}}$  spoils the asymmetry of the events; thus one cannot go to as low  $p_{T\text{ cut}}$  as for purely forward collisions.

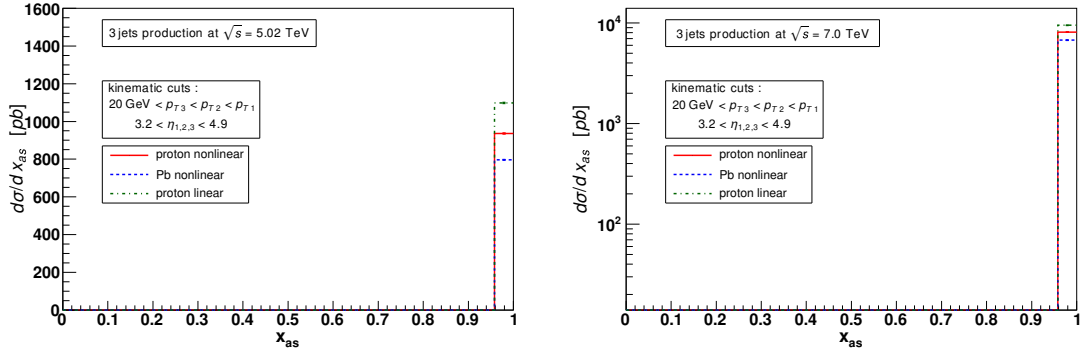


Figure 4: The differential cross section as a function of asymmetry variable  $x_{as}$  for purely forward rapidity region and two different c.m. energies: left for 5.02 TeV, right for 7.0 TeV.

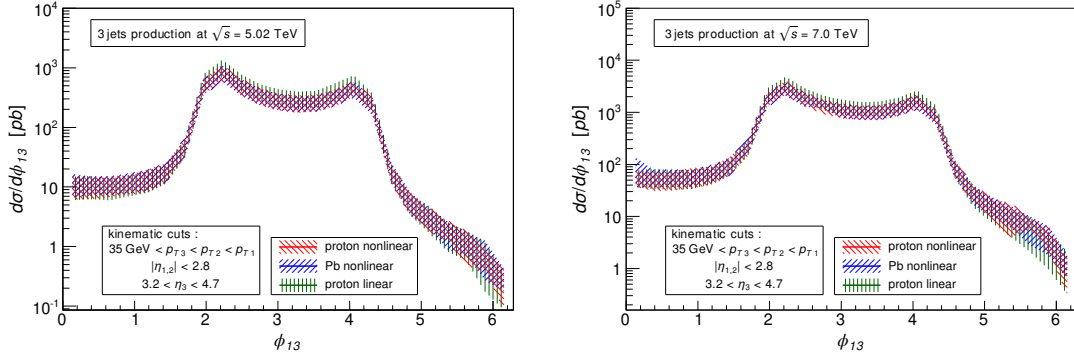


Figure 5: Differential cross section in difference of the azimuthal angles between the leading and forward jets. The band represents the theoretical uncertainty due to scale variation and statistical errors. The left plot corresponds to c.m. energy 5.02 TeV, the right to 7.0 TeV.

### 4.3 Azimuthal decorrelations

#### 4.3.1 Central-forward jets

Let us now present the results for azimuthal decorrelations for central-forward jet configuration. There are many azimuthal observables that can be studied within this context. In this paper we study distributions in the azimuthal angle between the leading jet (with index 1) and the softest jet (with index 3)

$$\phi_{13} = |\phi_1 - \phi_3|, \quad \phi_{13} \in [0, 2\pi]. \quad (19)$$

Note, that this angle is always calculated in one direction and is not just the smallest angle between the jets. This is important; if we assume that the direction of the leading jet divides the azimuthal plane to two half-planes, the events with the forward jet lying on the left half-plane and right-half-plane (with the same smallest angle to the leading jet) are not symmetric. Let us note that in the collinear factorization at leading order the momentum conservation requires that  $\pi/2 < \phi_{13} < 3\pi/2$ . Thus the shapes given in the plots discussed below are a characteristic feature of the high-energy factorization.

In Figs. 5-7 we present a sample of our result for the differential cross section in the variable  $\phi_{13}$ . We observe that indeed the whole region  $(0, 2\pi]$  is covered by events, however the “collinear” region  $\pi/2 < \phi_{13} < 3\pi/2$  dominates. The results for the nonlinear evolution described in the Section 2 for proton and lead, as well as the BFKL with sub leading corrections are similar and the nuclear modification ratio is consistent with unity, as seen in Fig. 6.

Let us now turn to the case when the two leading jets are restricted to be back-to-back-like. In the present calculation we choose  $D_{cut} = 30$  GeV. We have checked empirically that in order to observe any significant difference comparing to forward-central case discussed above we should use

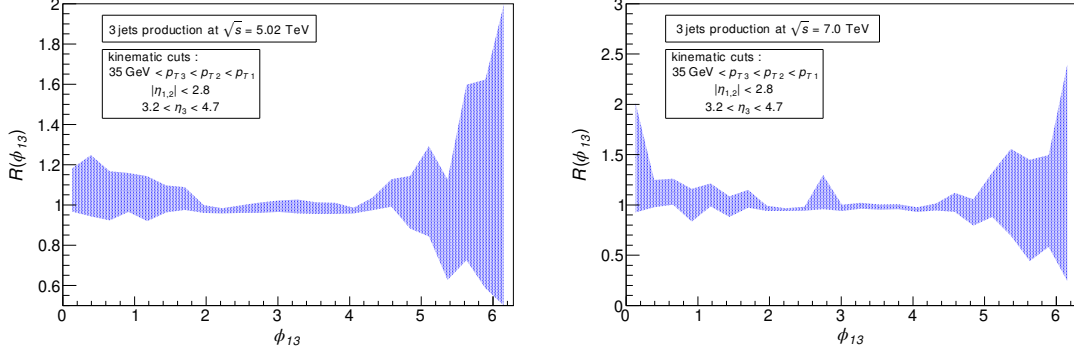


Figure 6: The nuclear modification factor as a function of difference of the azimuthal angles between the leading and forward jets. The band represents the theoretical uncertainty due to scale variation and statistical errors. The left plot corresponds to c.m. energy 5.02 TeV, the right to 7.0 TeV.

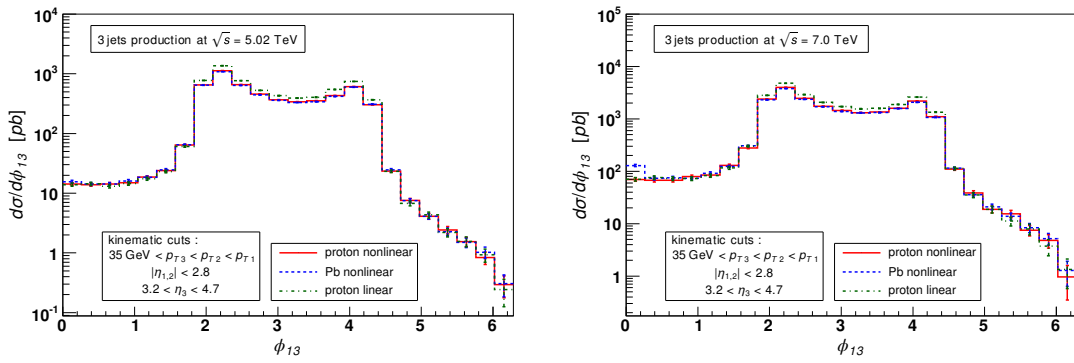


Figure 7: Differential cross section in difference of the azimuthal angles between the leading and forward jets for a particular choice of the scale  $\mu/2$ . The left column corresponds to c.m. energy 5.02 TeV, the right to 7.0 TeV.



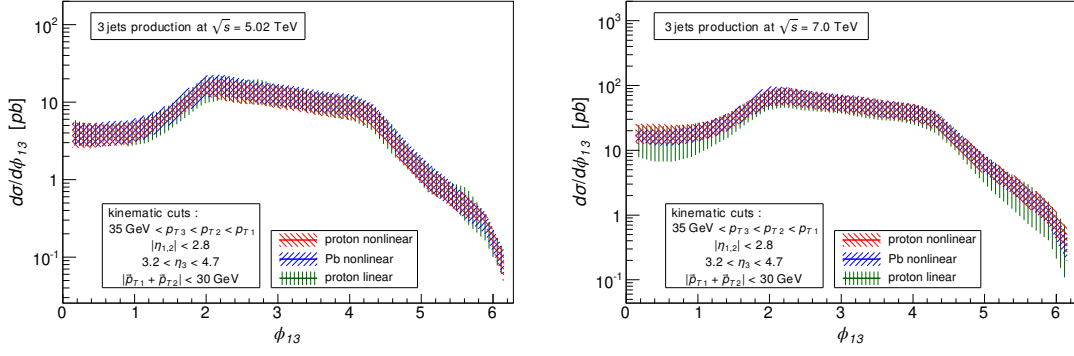


Figure 8: Differential cross section in difference of the azimuthal angles between the leading and forward jets with the additional restriction that the two leading jets are back-to-back-like. The band represents the theoretical uncertainty due to scale variation and statistical errors. The left plot corresponds to c.m. energy 5.02 TeV, the right to 7.0 TeV.

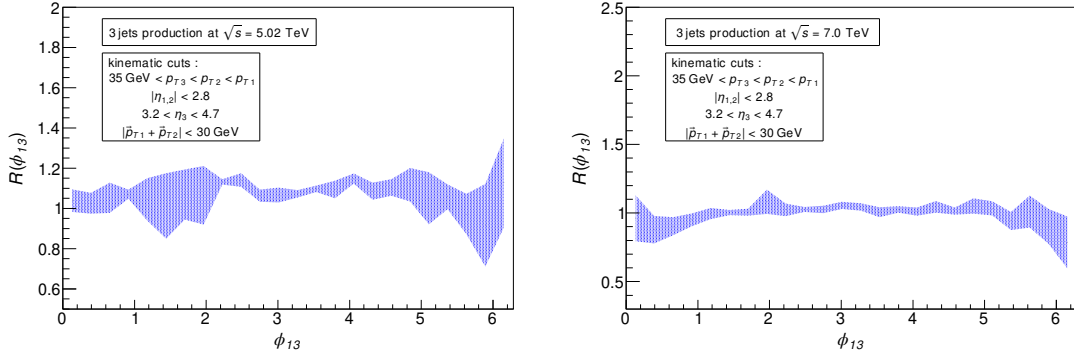


Figure 9: The nuclear modification factor as a function of difference of the azimuthal angles between the leading and forward jets, with the additional restriction that the two leading jets are back-to-back-like. The band represents the theoretical uncertainty due to scale variation and statistical errors. The left plot corresponds to c.m. energy 5.02 TeV, the right to 7.0 TeV.

$D_{\text{cut}} < p_{T\text{cut}}$ . Our results are presented in Figs. 8-10. The main properties of the distributions are the following. First, the relative magnitude between the “collinear” region and the “non-collinear” region is decreased comparing to the previous case. This indicates that we enter the region which is small  $x$  sensitive. We see (right of Figs. 8, 10) that for the c.m. energy of 7 TeV and large energy scale the distributions are different for linear and nonlinear evolution and the difference is most significant in the “noncollinear” region. The nuclear modification factor (Fig. 9) is, however, still consistent with unity.

#### 4.3.2 Forward jets

Let us move to the case where all of the jets are in the forward rapidity region. As discussed in Subsection 4.2, in this region we can safely go to relatively low values of  $p_{T\text{cut}}$ ; thus we set  $p_{T\text{cut}} = 20$  GeV. We present the results in Figs. 11-13. We observe significant differences between the three scenarios (nonlinear proton, nonlinear Pb and linear proton) in the middle region of  $\phi_{13}$  distributions, i.e. in the “collinear” region. It is also nicely illustrated by the nuclear modification ratios (Fig. 12) which now have two dips in that region, indicating that the region is sensitive to the nonlinear effects. The qualitative behavior is the same for both considered c.m. energies.

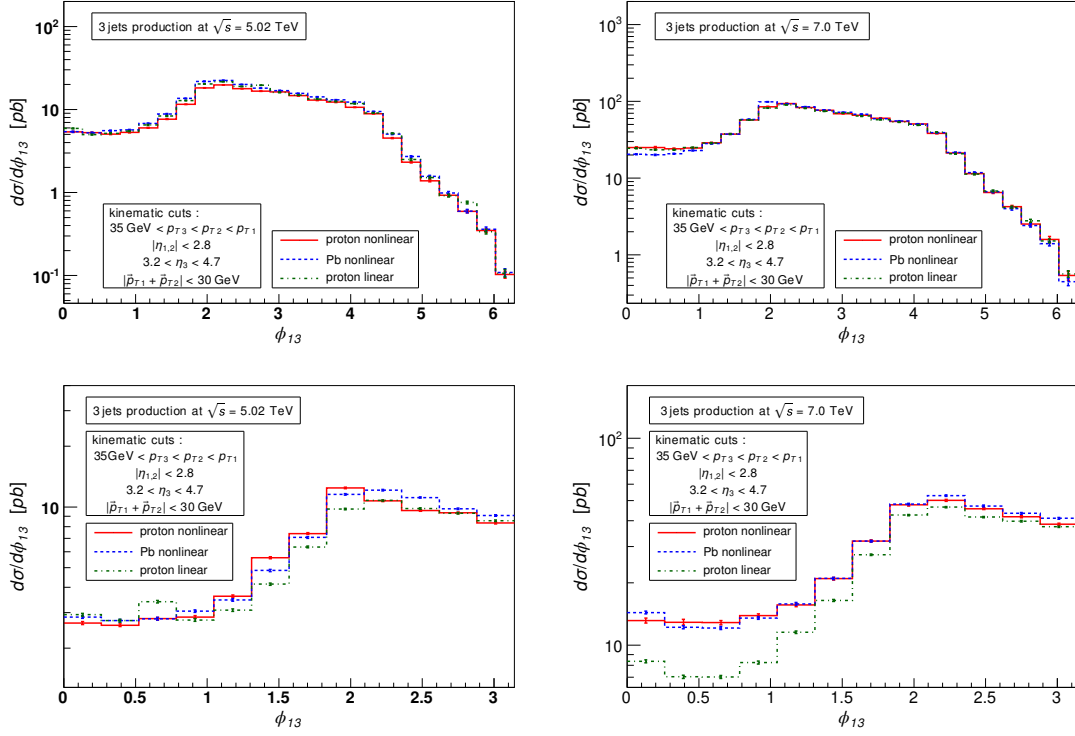


Figure 10: Differential cross section in difference of the azimuthal angles between the leading and forward jets, with the additional restriction that the two leading jets are back-to-back-like. The left column corresponds to c.m. energy 5.02 TeV, the right to 7.0 TeV. The top plots are made for the scale  $\mu/2$  while the bottom plots zoom the top plots for  $0 < \phi_{13} < \pi$  and are made for the scale  $2\mu$ .

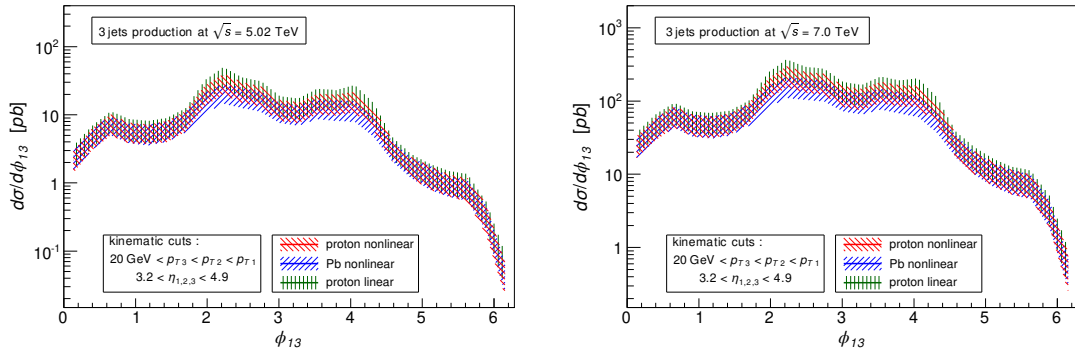


Figure 11: Differential cross section in difference of the azimuthal angles between the leading and forward jets for the forward rapidity region. The band represents the theoretical uncertainty due to scale variation and statistical errors. The left plot corresponds to c.m. energy 5.02 TeV, the right to 7.0 TeV.

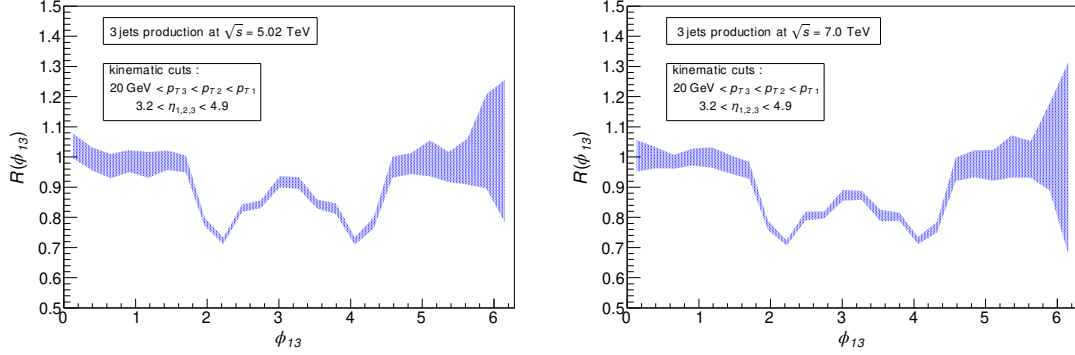


Figure 12: The nuclear modification factor as a function of difference of the azimuthal angles between the leading and forward jets for the forward rapidity region. The band represents the theoretical uncertainty due to scale variation and statistical errors. The left plot corresponds to c.m. energy 5.02 TeV, the right to 7.0 TeV.

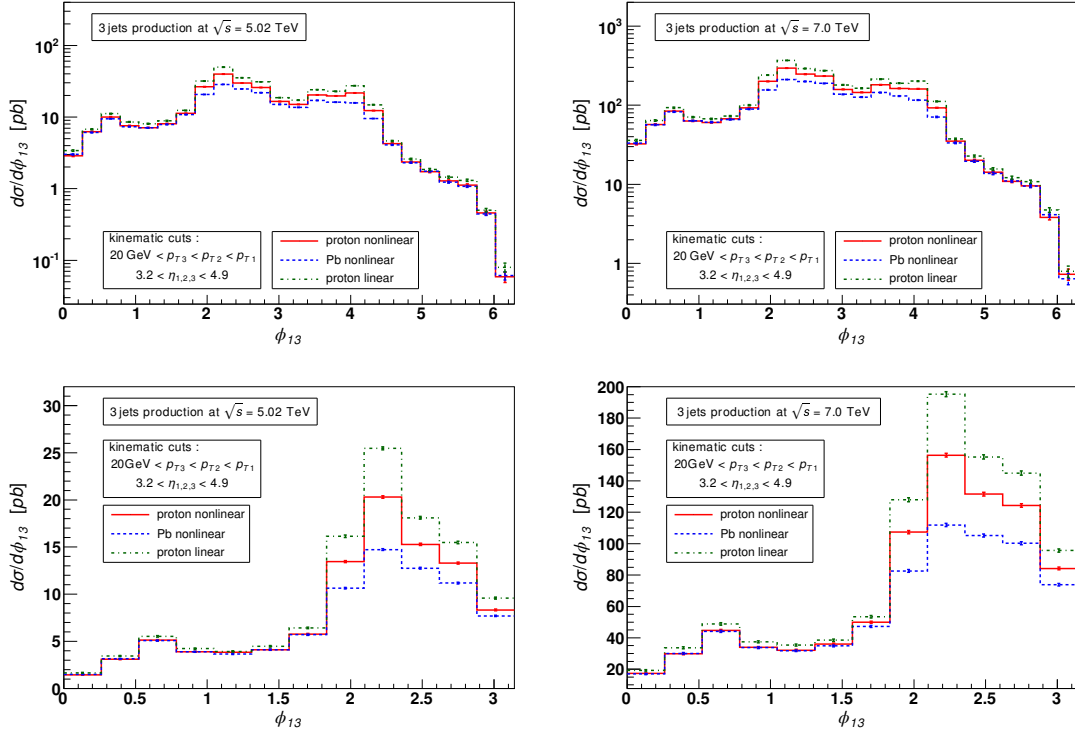


Figure 13: Differential cross section in difference of the azimuthal angles between the leading and forward jets for the forward rapidity region. The left column corresponds to c.m. energy 5.02 TeV, the right to 7.0 TeV. The top plots are made for the scale  $\mu/2$  while the bottom for the scale  $2\mu$  and  $0 < \phi_{13} < \pi$ .

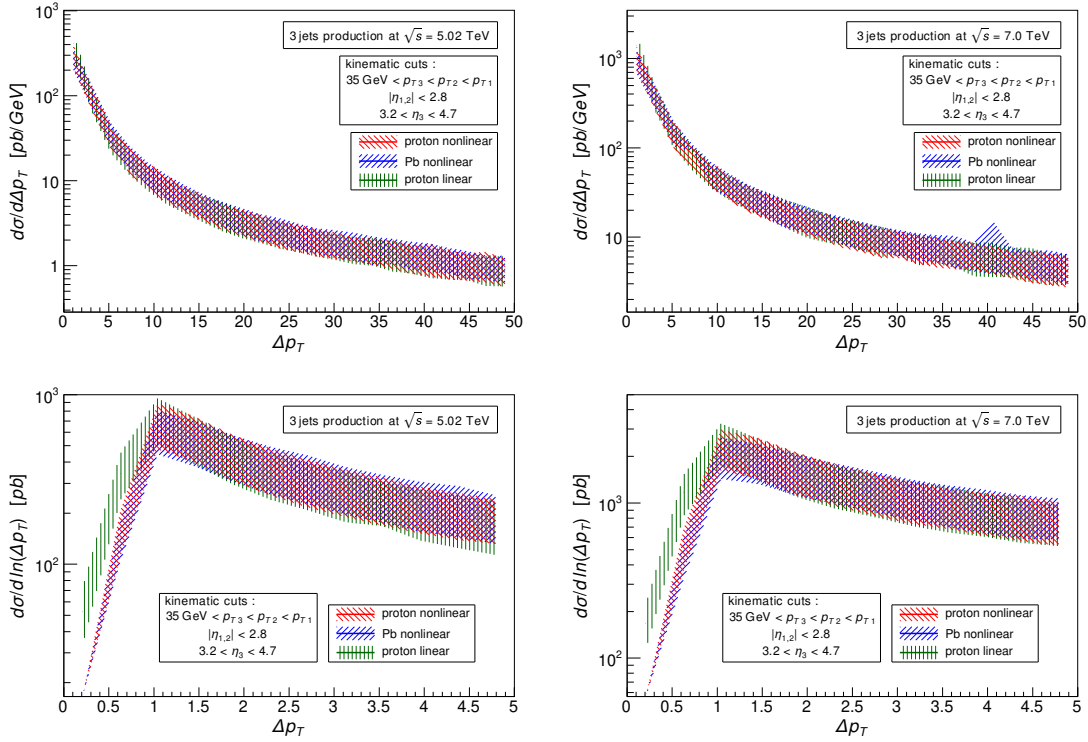


Figure 14: Differential cross section in the unbalanced  $p_T$  for central-forward jets. The band represents the theoretical uncertainty due to scale variation and statistical errors. The left plots correspond to c.m. energy 5.02 TeV, the right to 7.0 TeV. The bottom plots zoom the low  $\Delta p_T$  region (note the distributions are differential in  $\ln(\Delta p_T)$  there).

## 4.4 Unbalanced jet transverse momentum

Let us now switch to an analysis of the cross section as a function of the following quantity

$$\Delta p_T = |\vec{p}_{T1} + \vec{p}_{T2} + \vec{p}_{T3}|, \quad (20)$$

which in the prescription given by the Eq. (4) corresponds to the transverse momentum of the off-shell gluon, i.e.,  $\Delta p_T = |\vec{k}_{TA}|$ .

Let us remark, that the distributions we are going to present can be much more affected by the final state parton shower, than the decorrelation distribution presented above. Nevertheless, it is very interesting to study the influence of different evolution equations for the multiparticle production purely within the high-energy factorization.

### 4.4.1 Central-forward jets

We present the results in Figs. 14, 15, 16. The first immediate observation is that the distributions possess a maximum around 1 GeV (bottom of Figs. 14, 16) which corresponds to the maximum of the unintegrated gluon densities (see Ref. [46]) used in the calculations. The region below 1 GeV is sensitive to the different evolutions; the most significant difference is between linear and non-linear evolution, however the nuclear modification factor is slightly suppressed for  $\Delta p_T < 2.5$  GeV.

The scenario with the two leading jets being back-to-back-like is not especially interesting for the unbalanced transverse momentum distributions due to the kinematics involved. It turns out that the region of  $\Delta p_T$  that is smaller than a few GeV is kinematically forbidden. Although back-to-back forward-central jets probe actually the high transverse momenta in the unintegrated gluon density, we did not see any conclusive features of tails in our distributions.

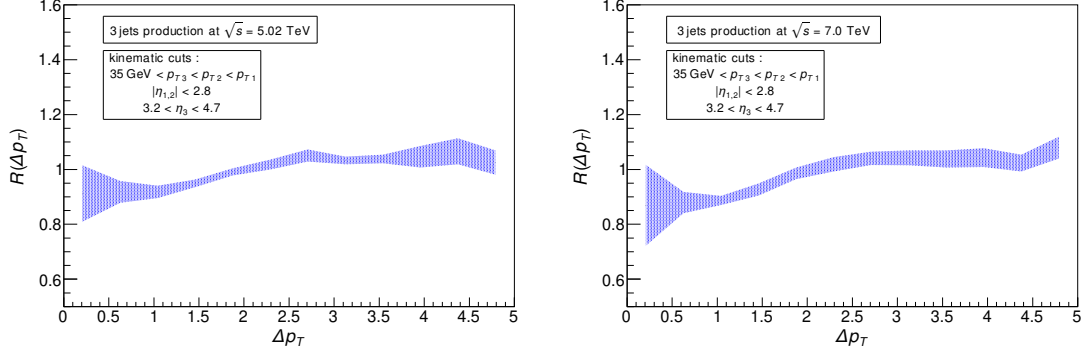


Figure 15: The nuclear modification factor for central-forward jets as a function of the unbalanced  $p_T$  for region close to zero. The band represents the theoretical uncertainty due to scale variation and statistical errors. The left plot corresponds to c.m. energy 5.02 TeV, the right to 7.0 TeV.

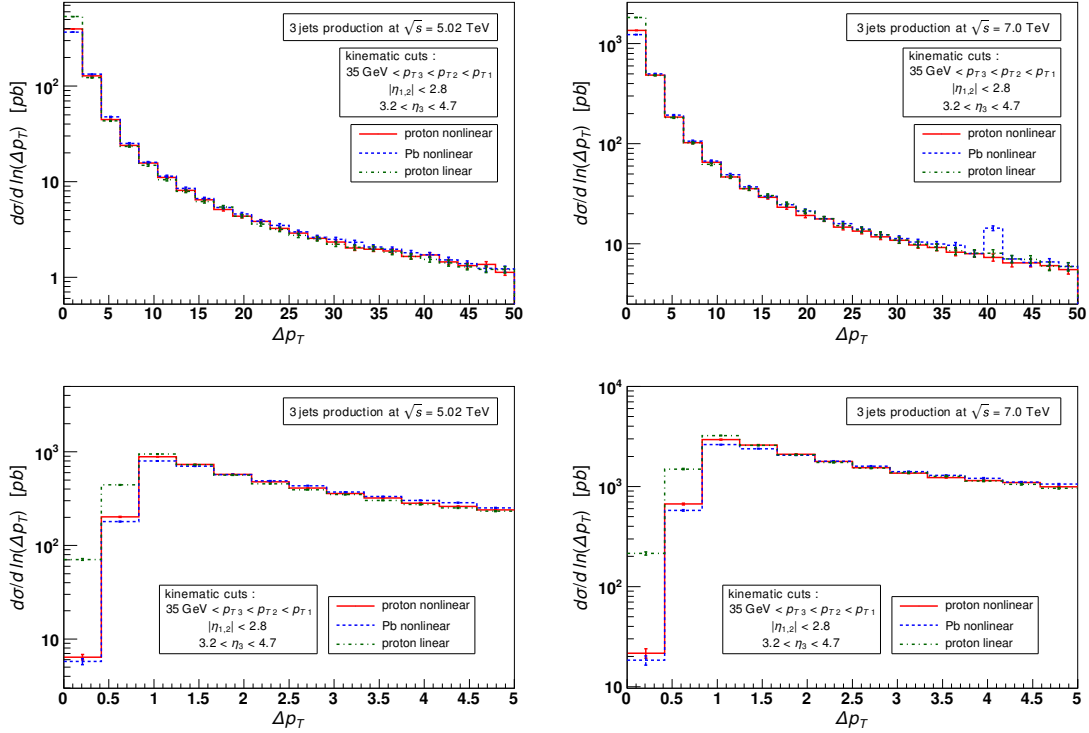


Figure 16: Differential cross section for central-forward jets in the unbalanced  $p_T$  for a particular choice of the scale  $\mu/2$ . The left column corresponds to c.m. energy 5.02 TeV, the right to 7.0 TeV. The bottom plots zoom the top plots for low  $\Delta p_T$  region but are calculated for the scale  $2\mu$  (note the distributions are in  $\ln(\Delta p_T)$  there).

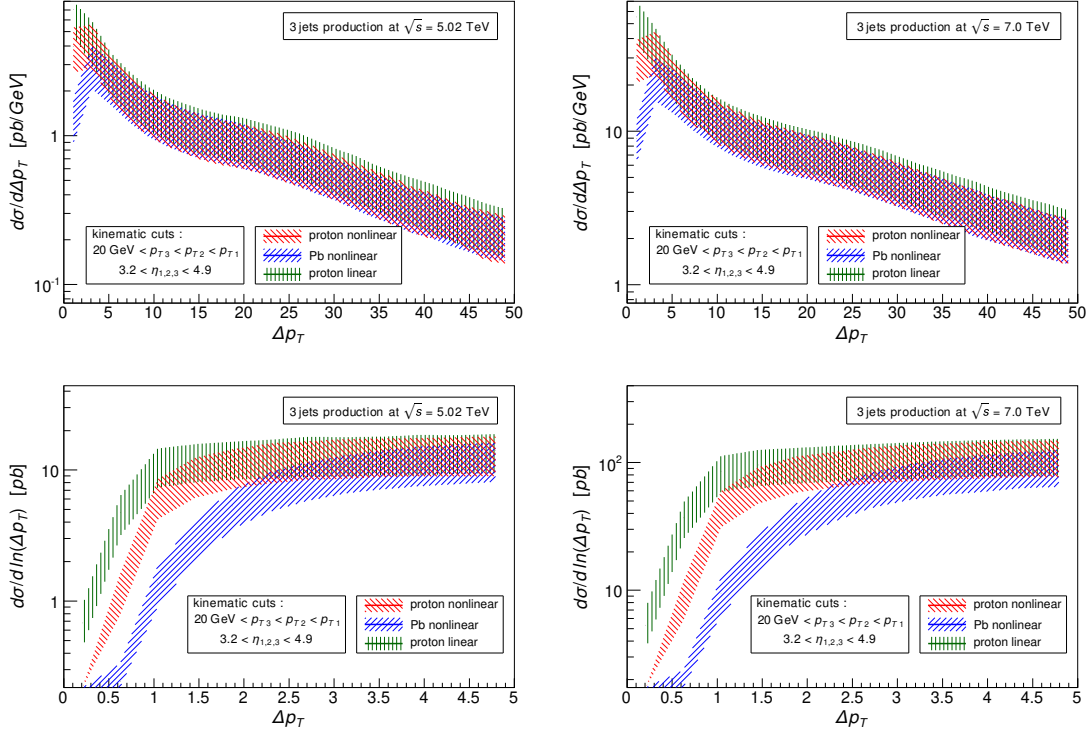


Figure 17: Differential cross section in the unbalanced  $p_T$  for forward jets. The band represents the theoretical uncertainty due to scale variation and statistical errors. The left plots correspond to c.m. energy 5.02 TeV, the right to 7.0 TeV. The bottom plots zoom the low  $\Delta p_T$  region (note the distributions are in  $\ln(\Delta p_T)$  there).

#### 4.4.2 Forward jets

Finally we turn to the forward rapidity region. Again we note the significant differences in the distributions for different evolution scenarios (Figs. 17-19). They are most prominent in the low unbalanced transverse momentum region  $\Delta p_T < 5$  GeV (see the bottom plots in Figs. 17-19). We note the suppression of the distributions with nonlinear evolution, with, however, lead being suppressed much more. This is also reflected in the nuclear modification ratios as is evident from Fig. 18. Interestingly, the nuclear modification factor is not so much sensitive to the scale variation.

## 5 Summary

In the present work we have studied three jet production at LHC for proton-proton and proton-lead collisions. As we pointed out the trijet final state is an ideal tool to perform scan of small  $x$  unintegrated gluon density and to discriminate between different evolution scenarios. In our work we have used two independent Monte Carlo programs which implement high-energy  $k_T$ -factorization with a single off-shell gluon and gauge invariant matrix elements. We have studied three scenarios for the evolution of the unintegrated gluon density: nonlinear evolution for proton and lead according to Refs. [45, 47] and its linear version. From numerous observables that can be constructed for a three jet process, we have chosen azimuthal decorrelations and the unbalanced transverse momentum of the jets. We considered two rapidity regions accessible experimentally: forward-central region and purely forward region. In addition we have considered the situation, when the two central jets are back-to-back-like. Our findings can be briefly summarized as follows. Forward-central collisions with relatively high cut on the transverse jet momenta are not sensitive to different kinds of gluon evolution, although they reflect some key features of the high-energy kinematics. The situation changes, when the two leading jets are approximately back-to-back as

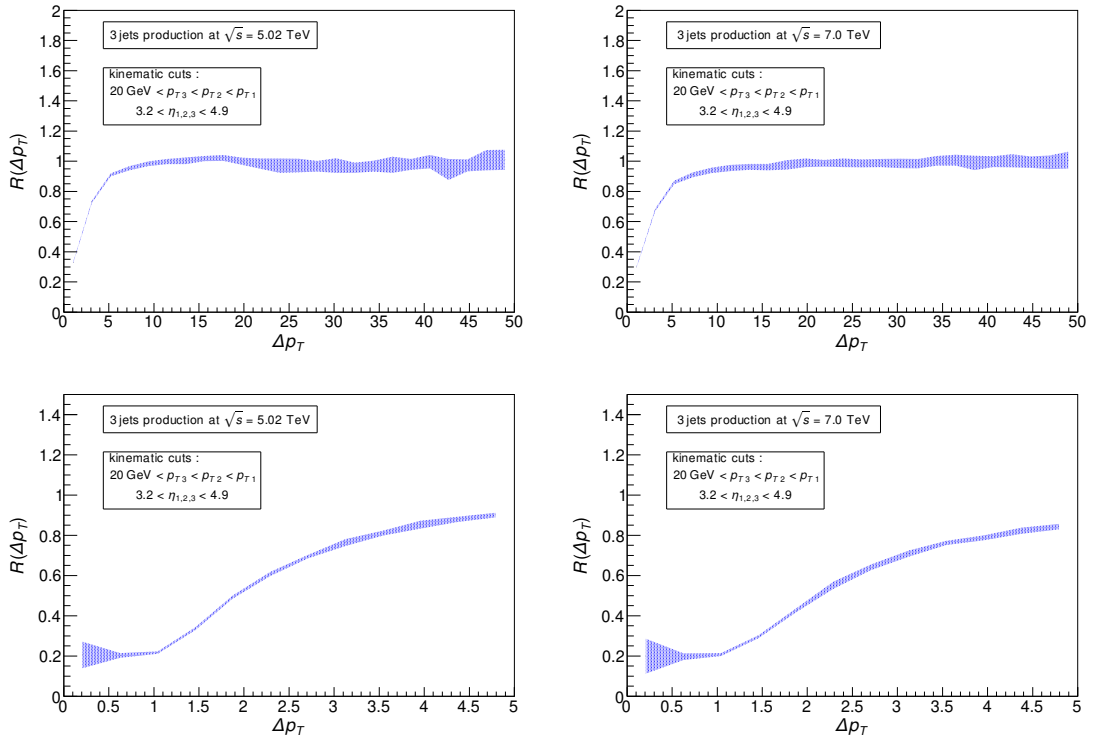


Figure 18: The nuclear modification factor for forward jets as a function of the unbalanced  $p_T$ . The band represents the theoretical uncertainty due to scale variation and statistical errors. The left plots correspond to c.m. energy 5.02 TeV, the right to 7.0 TeV. The bottom plots zoom the region close to zero.

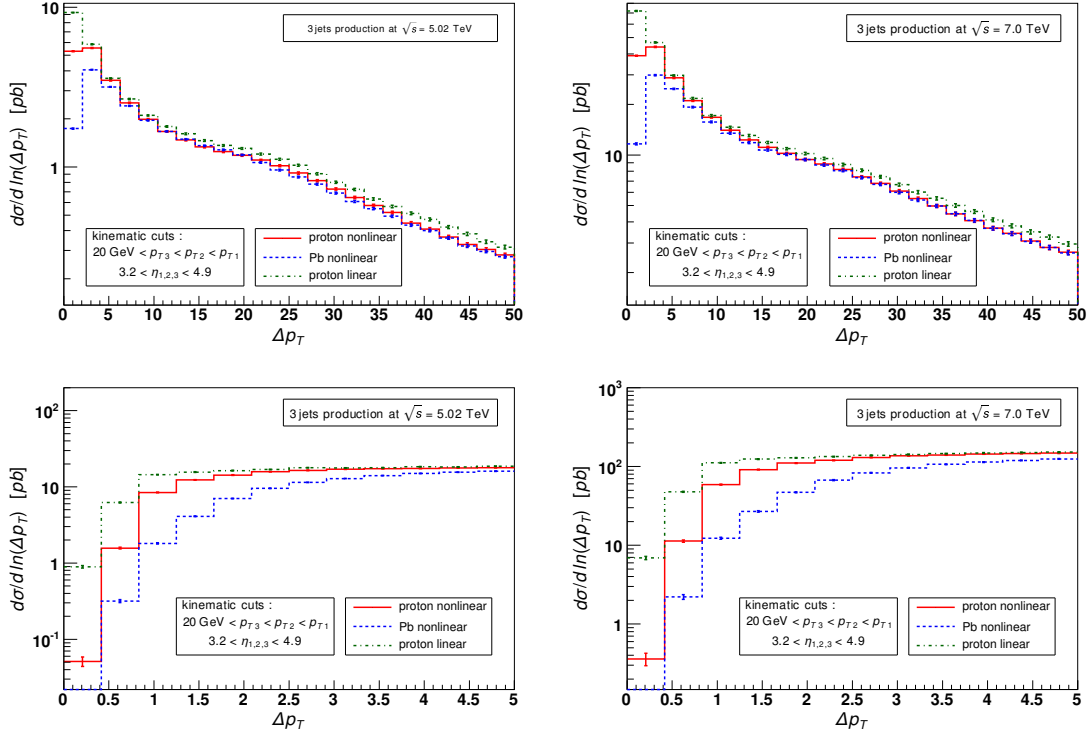


Figure 19: Differential cross section for forward jets in the unbalanced  $p_T$  for a particular choice of the scale  $\mu/2$ . The left column corresponds to c.m. energy 5.02 TeV, the right to 7.0 TeV. The bottom plots zoom the top plots for low  $\Delta p_T$  region (note the distributions are in  $\ln(\Delta p_T)$  there).

the distributions start to be sensitive to the region of a relatively large transverse momentum in the unintegrated gluon density. For the case of forward scattering, we observe significant difference between all three kinds of evolution, in particular the shape of the nuclear modification factors (Figs. 12, 18) suggest strong suppression due to saturation effects, which is visible both in the azimuthal decorrelations and the unbalanced  $p_T$  distributions.

## Acknowledgments

The authors are grateful N. Armesto, P. Cipriano, S. Jadach, P. van Mechelen, W. Słominski, M. Strikman, and M. Trzebiński for discussions.

This work was supported by the NCBiR grant LIDER/02/35/L-2/10/NCBiR/2011.

## References

- [1] J. L. Albacete and C. Marquet. Azimuthal correlations of forward di-hadrons in d+Au collisions at RHIC in the Color Glass Condensate. *Phys.Rev.Lett.*, 105:162301, 2010.
- [2] E. Antonov, L. Lipatov, E. Kuraev, and I. Cherednikov. Feynman rules for effective Regge action. *Nucl.Phys.*, B721:111–135, 2005.
- [3] E. Avsar. On the Understanding and Use of ‘Unintegrated’ Parton Distributions in Small-x QCD. *Int.J.Mod.Phys.Conf.Ser.*, 04:74–84, 2011.
- [4] E. Avsar. TMD factorization and the gluon distribution in high energy QCD. 2012.
- [5] I. Balitsky. Operator expansion for high-energy scattering. *Nucl.Phys.*, B463:99–160, 1996.



- [6] I. Balitsky and L. Lipatov. The Pomeron singularity in Quantum Chromodynamics. *Sov.J.Nucl.Phys.*, 28:822–829, 1978.
- [7] J. P. Blaizot, F. Gelis, and R. Venugopalan. High-energy pA collisions in the color glass condensate approach. 1. Gluon production and the Cronin effect. *Nucl.Phys.*, A743:13–56, 2004.
- [8] M. Cacciari, G. P. Salam, and G. Soyez. The Anti-k(t) jet clustering algorithm. *JHEP*, 0804:063, 2008.
- [9] S. Catani, M. Ciafaloni, and F. Hautmann. GLUON CONTRIBUTIONS TO SMALL  $x$  HEAVY FLAVOR PRODUCTION. *Phys.Lett.*, B242:97, 1990.
- [10] S. Catani, M. Ciafaloni, and F. Hautmann. High-energy factorization and small  $x$  heavy flavor production. *Nucl.Phys.*, B366:135–188, 1991.
- [11] S. Catani, M. Ciafaloni, and F. Hautmann. Small  $x$  structure functions and heavy flavor production. *Nucl.Phys.Proc.Suppl.*, 18C:220–225, 1991.
- [12] S. Catani, M. Ciafaloni, and F. Hautmann. High-energy factorization in QCD and minimal subtraction scheme. *Phys.Lett.*, B307:147–153, 1993.
- [13] S. Catani, F. Fiorani, and G. Marchesini. QCD Coherence in Initial State Radiation. *Phys.Lett.*, B234:339, 1990.
- [14] S. Catani, F. Fiorani, and G. Marchesini. Small  $x$  Behavior of Initial State Radiation in Perturbative QCD. *Nucl.Phys.*, B336:18, 1990.
- [15] S. Catani and F. Hautmann. Quark anomalous dimensions at small  $x$ . *Phys.Lett.*, B315:157–163, 1993.
- [16] S. Catani and F. Hautmann. High-energy factorization and small  $x$  deep inelastic scattering beyond leading order. *Nucl.Phys.*, B427:475–524, 1994.
- [17] G. Chachamis, M. Hentschinski, J. Madrigal Martinez, and A. S. Vera. Forward jet production and quantum corrections to the gluon Regge trajectory from Lipatov’s high energy effective action. 2012.
- [18] S. Chatrchyan et al. Measurement of energy flow at large pseudorapidities in  $pp$  collisions at  $\sqrt{s} = 0.9$  and 7 TeV. *JHEP*, 1111:148, 2011.
- [19] S. Chatrchyan et al. Measurement of the inclusive production cross sections for forward jets and for dijet events with one forward and one central jet in  $pp$  collisions at  $\sqrt{s} = 7$  TeV. *JHEP*, 1206:036, 2012.
- [20] M. Ciafaloni. Coherence Effects in Initial Jets at Small  $q^2 / s$ . *Nucl.Phys.*, B296:49, 1988.
- [21] J. Collins. *Foundations of perturbative QCD*, volume 32. Cambridge Univ. Press, 2011.
- [22] J. Collins and J.-W. Qiu.  $k_T$  factorization is violated in production of high-transverse-momentum particles in hadron-hadron collisions. *Phys.Rev.*, D75:114014, 2007.
- [23] M. Deak, F. Hautmann, H. Jung, and K. Kutak. Forward Jet Production at the Large Hadron Collider. *JHEP*, 0909:121, 2009.
- [24] M. Deak, F. Hautmann, H. Jung, and K. Kutak. Forward Jets and Energy Flow in Hadronic Collisions. *Eur.Phys.J.*, C72:1982, 2012.
- [25] V. Del Duca, M. E. Peskin, and W.-K. Tang. Computation of mini - jet inclusive cross-sections. *Phys.Lett.*, B306:151–157, 1993.
- [26] F. Dominguez, C. Marquet, A. M. Stasto, and B.-W. Xiao. Universality of multi-particle production in QCD at high energies. *Phys.Rev.*, D87:034007, 2013.

- [27] F. Dominguez, C. Marquet, B.-W. Xiao, and F. Yuan. Universality of Unintegrated Gluon Distributions at small  $x$ . *Phys.Rev.*, D83:105005, 2011.
- [28] A. Dumitru, K. Dusling, F. Gelis, J. Jalilian-Marian, T. Lappi, et al. The Ridge in proton-proton collisions at the LHC. *Phys.Lett.*, B697:21–25, 2011.
- [29] A. Dumitru, A. Hayashigaki, and J. Jalilian-Marian. The Color glass condensate and hadron production in the forward region. *Nucl.Phys.*, A765:464–482, 2006.
- [30] H. Fujii, F. Gelis, and R. Venugopalan. Quark pair production in high energy pA collisions: General features. *Nucl.Phys.*, A780:146–174, 2006.
- [31] F. Gelis, E. Iancu, J. Jalilian-Marian, and R. Venugopalan. The Color Glass Condensate. *Ann.Rev.Nucl.Part.Sci.*, 60:463–489, 2010.
- [32] L. Gribov, E. Levin, and M. Ryskin. Semihard Processes in QCD. *Phys.Rept.*, 100:1–150, 1983.
- [33] M. Hentschinski and C. Salas. Forward Drell-Yan plus backward jet as a test of BFKL evolution. pages 199–202, 2012.
- [34] E. Iancu and D. Triantafyllopoulos. JIMWLK evolution for multi-particle production in Langevin form. 2013.
- [35] D. Y. Ivanov and A. Papa. The next-to-leading order forward jet vertex in the small-cone approximation. *JHEP*, 1205:086, 2012.
- [36] S. Jadach. Foam: A General purpose cellular Monte Carlo event generator. *Comput.Phys.Commun.*, 152:55–100, 2003.
- [37] V. Khachatryan et al. Dijet Azimuthal Decorrelations in  $pp$  Collisions at  $\sqrt{s} = 7$  TeV. *Phys.Rev.Lett.*, 106:122003, 2011.
- [38] D. Kharzeev, Y. V. Kovchegov, and K. Tuchin. Cronin effect and high  $p(T)$  suppression in pA collisions. *Phys.Rev.*, D68:094013, 2003.
- [39] B. Kniehl, V. Saleev, A. Shipilova, and E. Yatsenko. Single jet and prompt-photon inclusive production with multi-Regge kinematics: From Tevatron to LHC. *Phys.Rev.*, D84:074017, 2011.
- [40] Y. V. Kovchegov. Small  $x$   $F(2)$  structure function of a nucleus including multiple pomeron exchanges. *Phys.Rev.*, D60:034008, 1999.
- [41] Y. V. Kovchegov and K. Tuchin. Inclusive gluon production in DIS at high parton density. *Phys.Rev.*, D65:074026, 2002.
- [42] E. Kuraev, L. Lipatov, and V. S. Fadin. The Pomeranchuk Singularity in Nonabelian Gauge Theories. *Sov.Phys.JETP*, 45:199–204, 1977.
- [43] K. Kutak. Resummation in nonlinear equation for high energy factorisable gluon density and its extension to include coherence. 2012.
- [44] K. Kutak, K. Golec-Biernat, S. Jadach, and M. Skrzypek. Nonlinear equation for coherent gluon emission. *JHEP*, 1202:117, 2012.
- [45] K. Kutak and J. Kwiecinski. Screening effects in the ultrahigh-energy neutrino interactions. *Eur.Phys.J.*, C29:521, 2003.
- [46] K. Kutak and S. Sapeta. Gluon saturation in dijet production in p-Pb collisions at Large Hadron Collider. *Phys.Rev.*, D86:094043, 2012.
- [47] K. Kutak and A. Stasto. Unintegrated gluon distribution from modified BK equation. *Eur.Phys.J.*, C41:343–351, 2005.

- [48] J. Kwiecinski, A. D. Martin, and A. Stasto. A Unified BFKL and GLAP description of F2 data. *Phys.Rev.*, D56:3991–4006, 1997.
- [49] H.-L. Lai, M. Guzzi, J. Huston, Z. Li, P. M. Nadolsky, et al. New parton distributions for collider physics. *Phys.Rev.*, D82:074024, 2010.
- [50] L. Lipatov. Gauge invariant effective action for high-energy processes in QCD. *Nucl.Phys.*, B452:369–400, 1995.
- [51] C. Marquet and C. Royon. Small-x QCD effects in forward-jet and Mueller-Navelet jet production. *Nucl.Phys.*, B739:131–155, 2006.
- [52] L. D. McLerran and R. Venugopalan. Computing quark and gluon distribution functions for very large nuclei. *Phys.Rev.*, D49:2233–2241, 1994.
- [53] L. D. McLerran and R. Venugopalan. Gluon distribution functions for very large nuclei at small transverse momentum. *Phys.Rev.*, D49:3352–3355, 1994.
- [54] A. H. Mueller and H. Navelet. An Inclusive Minijet Cross-Section and the Bare Pomeron in QCD. *Nucl.Phys.*, B282:727, 1987.
- [55] A. H. Mueller and J.-w. Qiu. Gluon Recombination and Shadowing at Small Values of x. *Nucl.Phys.*, B268:427, 1986.
- [56] P. Mulders and T. Rogers. Gauge Links, TMD-Factorization, and TMD-Factorization Breaking. 2011.
- [57] M. Nefedov, V. Saleev, and A. V. Shipilova. Dijet azimuthal decorrelations at the LHC in the parton Reggeization approach. *Phys.Rev.*, D87:094030, 2013.
- [58] T. C. Rogers and P. J. Mulders. No Generalized TMD-Factorization in Hadro-Production of High Transverse Momentum Hadrons. *Phys.Rev.*, D81:094006, 2010.
- [59] V. Saleev and A. Shipilova. Inclusive b-jet and  $b\bar{b}$ -dijet production at the LHC via Reggeized gluons. *Phys.Rev.*, D86:034032, 2012.
- [60] T. Sjostrand, S. Mrenna, and P. Z. Skands. A Brief Introduction to PYTHIA 8.1. *Comput.Phys.Comm.*, 178:852–867, 2008.
- [61] A. Stasto, K. J. Golec-Biernat, and J. Kwiecinski. Geometric scaling for the total  $\gamma^* p$  cross-section in the low x region. *Phys.Rev.Lett.*, 86:596–599, 2001.
- [62] A. Stasto, B.-W. Xiao, and F. Yuan. Back-to-Back Correlations of Di-hadrons in dAu Collisions at RHIC. *Phys.Lett.*, B716:430–434, 2012.
- [63] W. J. Stirling. Production of jet pairs at large relative rapidity in hadron hadron collisions as a probe of the perturbative pomeron. *Nucl.Phys.*, B423:56–79, 1994.
- [64] A. van Hameren, P. Kotko, and K. Kutak. Multi-gluon helicity amplitudes with one off-shell leg within high energy factorization. *JHEP*, 1212:029, 2012.
- [65] A. van Hameren, P. Kotko, and K. Kutak. Helicity amplitudes for high-energy scattering. *JHEP*, 1301:078, 2013.
- [66] B.-W. Xiao and F. Yuan. Non-Universality of Transverse Momentum Dependent Parton Distributions at Small-x. *Phys.Rev.Lett.*, 105:062001, 2010.

# Erratum: Three jet production and gluon saturation effects in p-p and p-Pb collisions within high-energy factorization

A. van Hameren, P. Kotko, K. Kutak

The H. Niewodniczański Institute of Nuclear Physics

Polish Academy of Sciences

Radzikowskiego 152, 31-342 Cracow, Poland

The following erratum updates the results for the azimuthal decorrelations published in our original work. There, the decorrelations were defined as differential cross sections in the following variable

$$\phi_{13} = |\phi_1 - \phi_3|, \quad \phi_{1,3} \in [0, 2\pi), \quad (1)$$

where  $\phi_1, \phi_3$  are azimuthal positions of the leading and softest jets respectively (the hardness is defined according to the jets transverse momentum). As we commented in the section entitled "Azimuthal decorrelations", due to such definition of  $\phi_{13}$  the distributions are not mirror-symmetric with respect to  $\phi_{13} = \pi$  axis. Since this asymmetry is unphysical we recalculate the azimuthal decorrelations using  $\phi_{13}$  defined as the *smallest azimuthal angle* between the leading and the softest jets. The new plots are presented in figures below and they update Figs. 5-13 of the original work.

We would like to thank L. Lönnblad, P. van Mechelen and A. Szczurek for discussions regarding the issue.

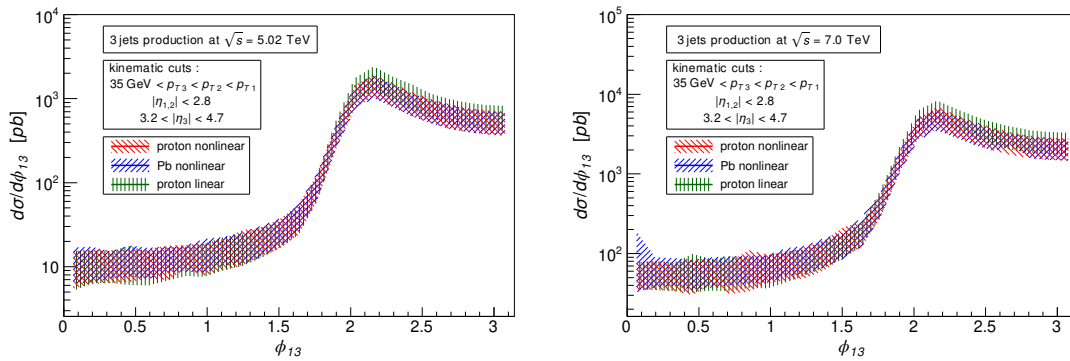


Figure 1: Differential cross section in difference of the azimuthal angles between the leading and forward jets. The band represents the theoretical uncertainty due to scale variation and statistical errors. The left plot corresponds to c.m. energy 5.02 TeV, the right to 7.0 TeV.

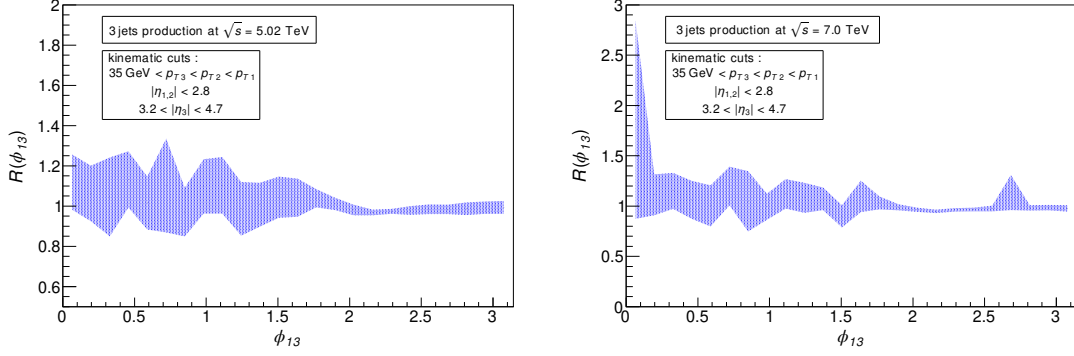


Figure 2: The nuclear modification factor as a function of difference of the azimuthal angles between the leading and forward jets. The band represents the theoretical uncertainty due to scale variation and statistical errors. The left plot corresponds to c.m. energy 5.02 TeV, the right to 7.0 TeV.

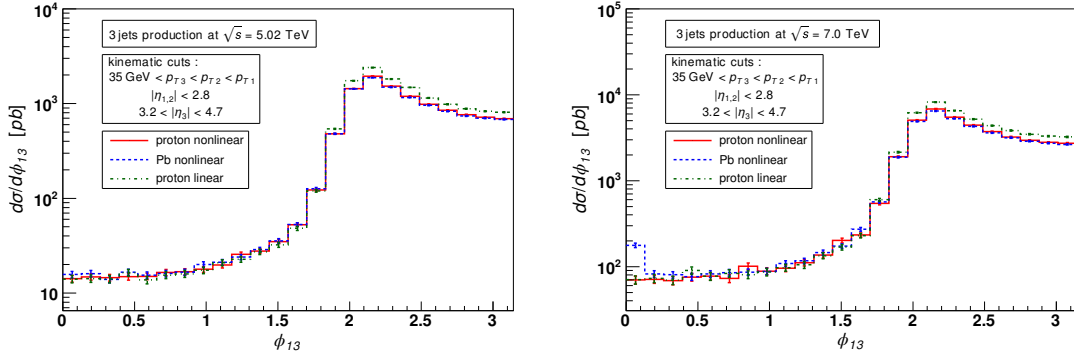


Figure 3: Differential cross section in difference of the azimuthal angles between the leading and forward jets for a particular choice of the scale  $\mu/2$ . The left column corresponds to c.m. energy 5.02 TeV, the right to 7.0 TeV.

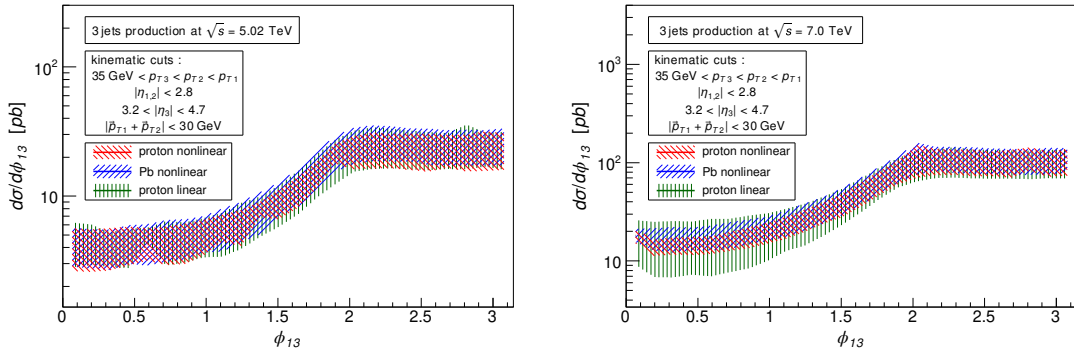


Figure 4: Differential cross section in difference of the azimuthal angles between the leading and forward jets with the additional restriction that the two leading jets are back-to-back-like. The band represents the theoretical uncertainty due to scale variation and statistical errors. The left plot corresponds to c.m. energy 5.02 TeV, the right to 7.0 TeV.

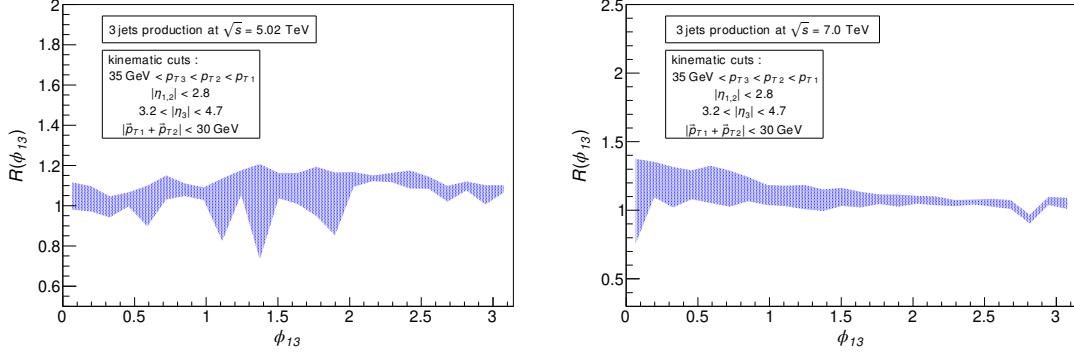


Figure 5: The nuclear modification factor as a function of difference of the azimuthal angles between the leading and forward jets, with the additional restriction that the two leading jets are back-to-back-like. The band represents the theoretical uncertainty due to scale variation and statistical errors. The left plot corresponds to c.m. energy 5.02 TeV, the right to 7.0 TeV.

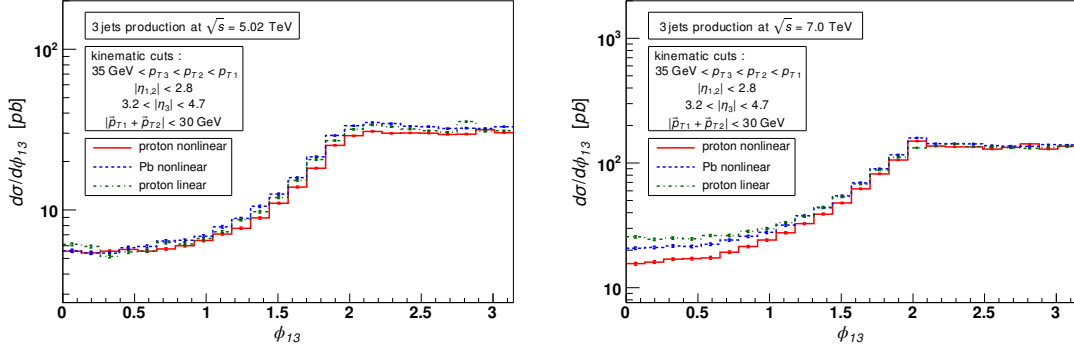


Figure 6: Differential cross section in difference of the azimuthal angles between the leading and forward jets, with the additional restriction that the two leading jets are back-to-back-like. The left plot corresponds to c.m. energy 5.02 TeV, the right to 7.0 TeV. The plots are made for the particular choice of the scale equal to  $\mu/2$ .

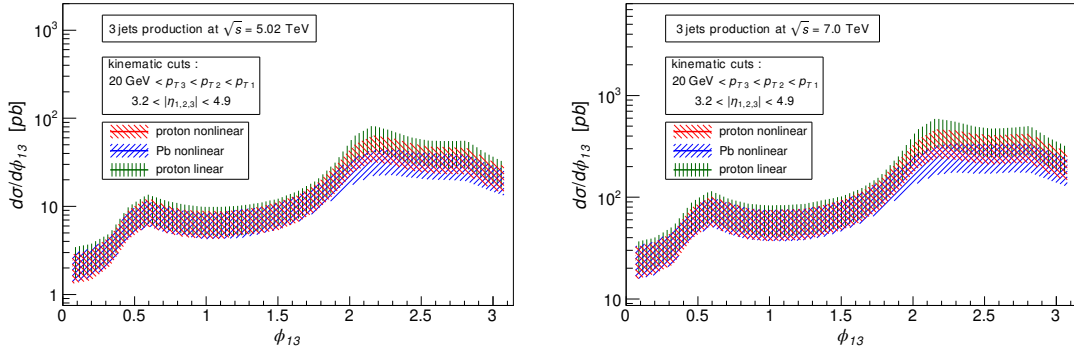


Figure 7: Differential cross section in difference of the azimuthal angles between the leading and forward jets for the forward rapidity region. The band represents the theoretical uncertainty due to scale variation and statistical errors. The left plot corresponds to c.m. energy 5.02 TeV, the right to 7.0 TeV.

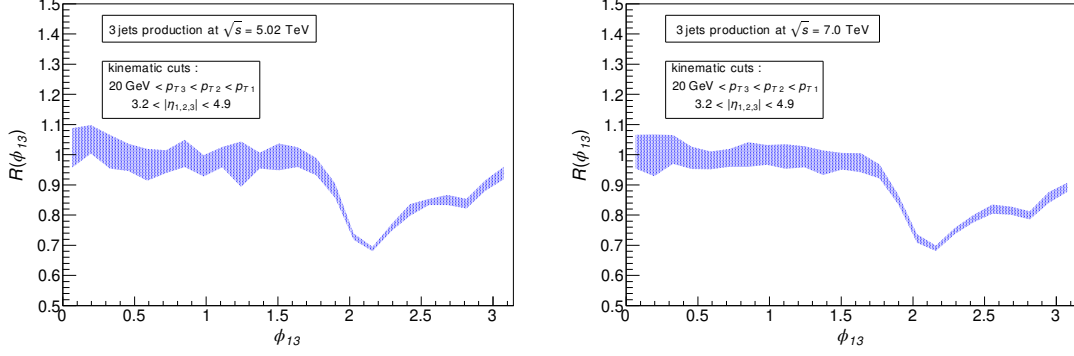


Figure 8: The nuclear modification factor as a function of difference of the azimuthal angles between the leading and forward jets for the forward rapidity region. The band represents the theoretical uncertainty due to scale variation and statistical errors. The left plot corresponds to c.m. energy 5.02 TeV, the right to 7.0 TeV.

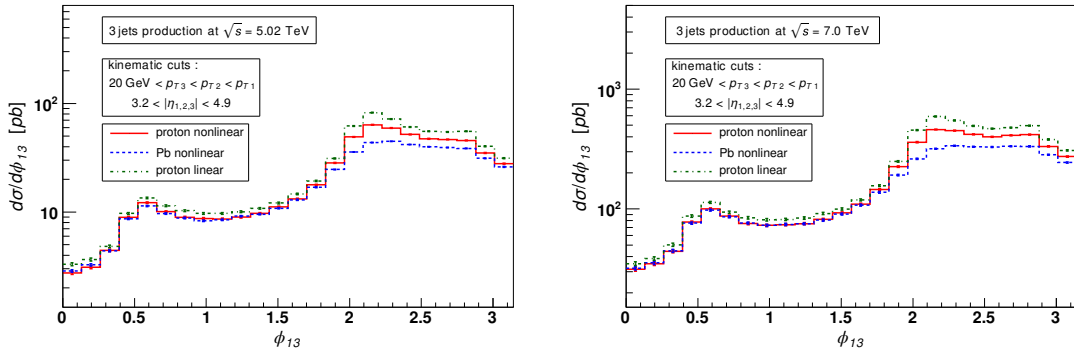


Figure 9: Differential cross section in difference of the azimuthal angles between the leading and forward jets for the forward rapidity region. The left plot corresponds to c.m. energy 5.02 TeV, the right to 7.0 TeV. The plots are made for the particular choice of the scale equal to  $\mu/2$ .